# *N*-Benzoylpyrazoles Are Novel Small-Molecule Inhibitors of Human Neutrophil Elastase

Igor A. Schepetkin,[†] Andrei I. Khlebnikov,[‡] and Mark T. Quinn*[,†]

*Department of Veterinary Molecular Biology, Montana State University, Bozeman, Montana 59717, and Department of Chemistry, Altai State Technical University, Barnaul 656038, Russia*

*Received May 22, 2007*

Human neutrophil elastase (NE) plays an important role in the pathogenesis of pulmonary disease. Using high-throughput chemolibrary screening, we identified 10 *N*-benzoylpyrazole derivatives that were potent NE inhibitors. Nine additional NE inhibitors were identified through further screening of *N*-benzoylpyrazole analogues. Evaluation of inhibitory activity against a range of proteases showed high specificity for NE, although several derivatives were also potent inhibitors of chymotrypsin. Analysis of reaction kinetics and inhibitor stability revealed that *N*-benzoylpyrazoles were pseudoirreversible competitive inhibitors of NE. Structure−activity relationship (SAR) analysis demonstrated that modification of *N*-benzoylpyrazole ring substituents modulated enzyme selectivity and potency. Furthermore, molecular modeling of the binding of selected active and inactive compounds to the NE active site revealed that active compounds fit well into the catalytic site, whereas inactive derivatives contained substituents or conformations that hindered binding or accessibility to the catalytic residues. Thus, *N*-benzoylpyrazole derivatives represent novel structural templates that can be utilized for further development of efficacious NE inhibitors.

## Introduction

Acute respiratory distress syndrome (ARDS[a]), chronic obstructive pulmonary disease (COPD), and cystic fibrosis (CF) are progressive diseases that are frequently fatal.[1−3] Unfortunately, there are currently few effective therapeutic treatments for these syndromes. Inflammation associated with these pulmonary diseases is predominantly due to neutrophils and is associated with excessive release of neutrophil granule proteases, such as neutrophil elastase (NE, EC 3.4.21.37).[4,5] NE is a serine protease that is synthesized in neutrophils and stored in azurophilic granules.[6] While the primary role of NE appears to be in microbial killing in the phagosome, excessive NE release into extracellular fluids can cause major tissue damage.[7] For example, NE is released in large amounts during pulmonary inflammation, resulting in a protease/antiprotease imbalance, and this imbalance appears to be a major pathogenic determinant in COPD and ARDS.[5,8−10]

NE is a member of the chymotrypsin family of serine proteases and is expressed primarily in neutrophils but is also present in monocytes and mast cells. It can degrade a variety of extracellular matrix proteins, including elastin, fibronectin, laminin, collagen, and proteoglycans (reviewed in refs 11 and 12). NE also can activate several matrix metalloproteinases (MMP-2, -3, and -9)[13] and seems to play an important physiologic role in tissue repair through its ability to regulate growth factors and modulate cytokine expression at epithelial and endothelial surfaces.[14,15] However, excessive NE activity can lead to severe pathology through the degradation of elastin and collagen in the airways, resulting in microvascular injury and interstitial edema.[16]

Given the destructive potential of unregulated NE, it is not surprising that inhibition of NE activity in pulmonary tissues has been considered a promising strategy to improve the outcome of pulmonary diseases.[17,18] A number of therapeutic strategies have focused on the use of recombinant or purified preparations of two endogenous NE inhibitors described above, $\alpha_1$-antitrypsin and secretory leukocyte protease inhibitor; however, use of these inhibitors has been problematic.[19] Many types of peptide and nonpeptide inhibitors, employing both reversible and irreversible mechanisms of action, have also been reported (reviewed in refs 15, 19, and 20). Among the most potent NE inhibitors are $\beta$-lactams,[21] *tert*-butyloxadiazoles,[22] and peptidyl trifluoromethyl ketones.[23] Nevertheless, the primary chemical scaffolds of the most potent NE inhibitors were discovered 15−20 years ago,[24,25] and modification of these scaffolds is still the current focus of most NE inhibitor development because moving away from these core scaffolds would be difficult and time-consuming.[26] Conversely, we propose that new NE inhibitors with different structural and/or physicochemical properties from those described so far could lead to novel and useful leads for the development of anti-inflammatory drugs. Although some novel approaches have been developed for high-throughput screening (HTS) to identify NE inhibitors on a large scale, there are still only a few reports on HTS of elastase inhibitors.[27−29] Thus, we utilized HTS of a chemical diversity library containing 10 000 druglike molecules to identify novel inhibitors of NE that have core structures distinct from currently known leads. Notably, the hits obtained from our screen included 10 *N*-benzoylpyrazole derivatives, which were potent NE inhibitors. Furthermore, analysis of 43 additional *N*-benzoylpyrazole derivatives resulted in the identification of nine more potent NE inhibitors with $K_i \leq 1\ \mu$M. Evaluation of target specificity showed that most of NE inhibitors were selective for NE and chymotrypsin but not other proteases tested. Finally, molecular modeling approaches demonstrated that active *N*-benzoylpyrazole derivatives were able to effectively dock within the NE catalytic site so that Michaelis complex formation and synchronous proton transfer were favored, while binding of inactive derivatives into the pocket was sterically hindered or catalytically unfavorable.

* To whom correspondence should be addressed. Phone: 406-994-5721. Fax: 406-994-4303. E-mail: mquinn@montana.edu.

[†] Montana State University.

[‡] Altai State Technical University.

[a] Abbreviations: ARDS, adult respiratory distress syndrome; COPD, chronic obstructive pulmonary disease; HTS, high-throughput screening; NE, neutrophil elastase; RP-HPLC, reverse-phase high-performance liquid chromatography.

10.1021/jm070600+ CCC: $37.00 
Published on Web 09/12/2007

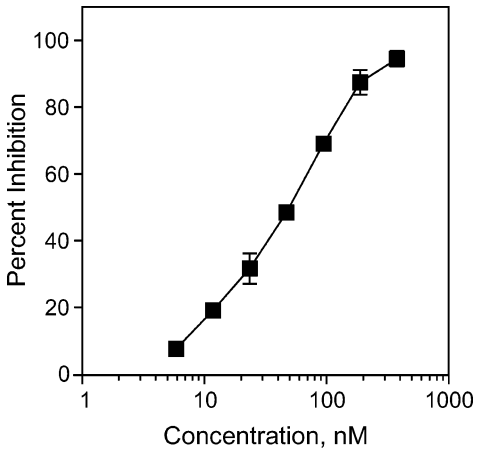


**Figure 1.** Inhibition of NE activity by a representative compound identified with HTS. NE was incubated with the indicated concentrations of **7**, and cleavage of the fluorogenic NE substrate (25 $\mu$M) was monitored, as described. The percent inhibition of NE activity is plotted vs the logarithm of inhibitor concentration. The data are presented as the mean ± SEM of triplicate samples from a representative experiment of three independent experiments.

## Results and Discussion

**Primary High-Throughput Screening.** To identify novel compounds that inhibit NE protease activity, we screened a chemical diversity library of 10 000 druglike compounds with molecular weights from 200 to 550 Da. This library of commonly accepted pharmaceutical hit structures was randomly assembled to maximize chemical diversity and includes 6118 compounds containing an amide linker. However, the library does not contain $\beta$-lactam derivatives, which have been reported previously as NE inhibitors.[21,30] Further details on the composition of the parent library are described in our previous studies.[31,32]

A compound was defined as a hit if it exhibited >90% inhibition of NE activity at a final compound concentration of 20 $\mu$g/mL in fluorescence-based microplate assays. From the primary enzymatic screening, 432 inhibitory compounds were selected (4.3% hit rate). The size of the hit set was further reduced by applying a series of experimental filters. For example, compounds that formed crystals or aggregates in aqueous buffer were eliminated, as they could inhibit enzymes nonspecifically by absorption of enzyme molecules to/into the aggregates.[33] We also determined the dose−response relationship for enzyme inhibition by hits filtered from the primary screen.[31,34] As an example, a representative curve for compound **7** is shown in Figure 1. Sixteen compounds with the highest inhibitory activity for NE were selected as a set of prospective NE inhibitors, and the inhibition constants ($K_i$) were determined for these compounds using Dixon plots.[35] The structures of these compounds and their activity are presented in Table 1. Compounds **1**−**10** were quite potent, all with $K_i \leq 110$ nM. This inhibition is likely not due to quenching of product fluorescence by the test compounds, as nanomolar concentrations of compounds do not appear to cause this problem.[36] In addition, we mixed selected lead compounds with cleaved substrate and found no effect on the fluorescence signal intensity at excitation and emission wavelengths of 355 and 460 nm, respectively (data not shown).

An examination of the 16 most potent NE inhibitors showed that 10 of these compounds (62%) had *N*-benzoylpyrazole scaffolds (Table 1). This scaffold has been reported among compounds with diuretic,[37] antidiabetic,[38] antivirus,[39] and anti-inflammatory[40] properties. However, to our knowledge, no other potent NE inhibitors have been reported to be *N*-benzoylpyrazole derivatives. Indeed, our findings suggest the possibility that the anti-inflammatory effects reported for *N*-benzoylpyrazoles[40] may be due, in part, to inhibition of NE. On the basis of this discovery, we selected 43 additional *N*-benzoylpyrazole derivatives from the TimTec stock library, which contains 224 700 compounds, for evaluation of NE inhibitory activity. All of these derivatives were soluble in aqueous buffer at the highest tested concentrations (50−55 $\mu$M), and dose−response analysis showed that eight of these compounds (compounds **17**−**24**) were relatively potent ($K_i \leq 300$ nM) NE inhibitors (Table 2 and Supporting Information Table S1). Thus, we selected the 17 most potent *N*-benzoylpyrazole derivatives (compounds **1**−**9** and **17**−**24**) for further characterization and SAR analysis. Dixon plots and double-reciprocal Lineweaver−Burk plots of substrate

**Table 1.** Chemical Structures and Inhibitory Activity of the Most Potent NE Inhibitors Identified by High-Throughput Screening

| compound | $K_i$ (nM) | structure | compound | $K_i$ (nM) | structure |
|---|---|---|---|---|---|
| **1** | 6 | 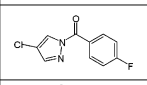 | **9** | 107 | 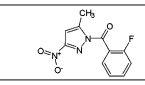 |
| **2** | 15 | 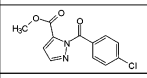 | **10** | 110 | 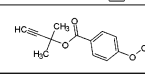 |
| **3** | 24 | 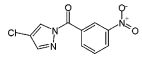 | **11** | 290 | 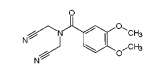 |
| **4** | 24 | 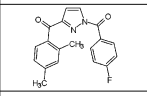 | **12** | 820 | 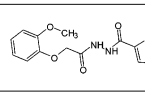 |
| **5** | 34 | 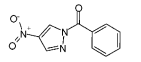 | **13** | 1100 | 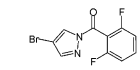 |
| **6** | 39 | 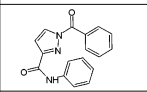 | **14** | 1600 | 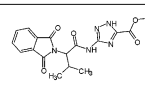 |
| **7** | 45 | 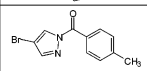 | **15** | 2500 | 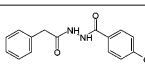 |
| **8** | 104 | 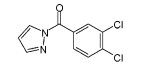 | **16** | 3100 | 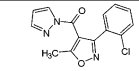 |

**Table 2.** Effect of *N*-Benzoylpyrazoles **17**−**33** on NE Activity[a]

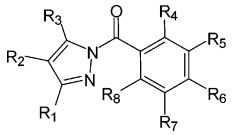

| compd | $R_1$ | $R_2$ | $R_3$ | $R_4$ | $R_5$ | $R_6$ | $R_7$ | $R_8$ | $K_i$ (nM) |
|---|---|---|---|---|---|---|---|---|---|
| **17** | $CH_3$ | H | H | H | $OCH_3$ | $OCH_3$ | $OCH_3$ | H | 21 |
| **18** | $NO_2$ | H | H | H | H | $CH_3$ | H | H | 28 |
| **19** | $NO_2$ | H | H | H | H | H | H | H | 46 |
| **20** | H | $NO_2$ | H | $CH_3$ | H | H | H | H | 65 |
| **21** | H | Cl | H | $CH_3$ | H | H | H | H | 230 |
| **22** | H | Br | H | H | $CH_3$ | H | H | H | 250 |
| **23** | H | Br | H | $CH_3$ | H | H | H | H | 300 |
| **24** | $CH_3$ | H | H | H | H | $NHCOCH_3$ | H | H | 300 |
| **25** | H | Cl | H | Cl | H | H | H | H | 1000 |
| **26** | H | H | H | $CH_3$ | H | H | H | H | 3400 |
| **27** | H | Br | H | H | F | F | H | Cl | 7200 |
| **28** | H | Cl | H | H | H | *tert*-butyl | H | H | 9000 |
| **29** | $CH_3$ | Cl | $CH_3$ | F | H | H | H | H | 9000 |
| **30** | $CH_3$ | Cl | $CH_3$ | H | H | Cl | H | H | 10700 |
| **31** | $CH_3$ | Br | $CH_3$ | H | H | $OCH_3$ | H | H | 24500 |
| **32** | H | H | H | Br | H | H | H | H | 29900 |
| **33** | $CH_3$ | $CH_3$ | $CH_3$ | H | $OCH_3$ | $OCH_3$ | $OCH_3$ | H | 50900 |

[a] See Supporting Information Table S1 for analysis results of compounds **34**−**59**.

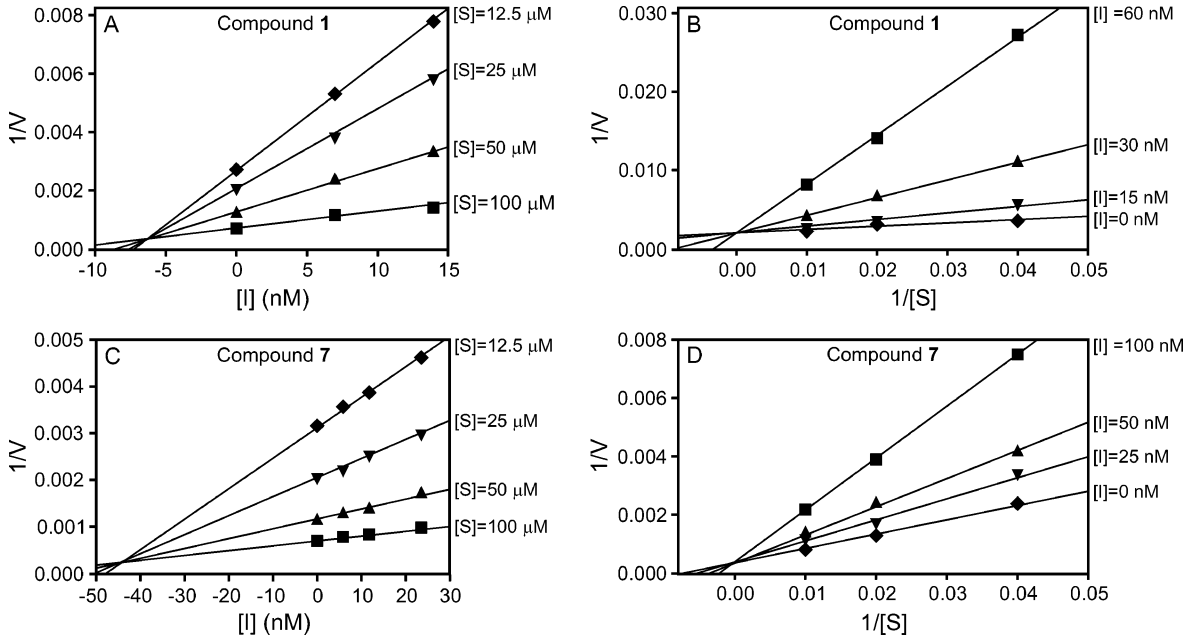


**Figure 2.** Kinetics of NE inhibition by selected *N*-benzoylpyrazole derivatives. Representative Dixon plots (A and C) and double-reciprocal Lineweaver−Burk plots (B and D) are shown. Representative plots are from three independent experiments.

hydrolysis by NE in the absence and presence of the selected compounds showed competitive inhibition (Figure 2 shows representative plots).

**Stability and Kinetic Features of *N*-Benzoylpyrazole Derivatives.** The set of 17 most potent NE inhibitors, as well as selected low activity and inactive *N*-benzoylpyrazoles, were evaluated for their chemical stability in aqueous buffer. Spontaneous hydrolysis rates and reaction orders of the inhibitors were measured in phosphate buffer at pH 7.3 and 25 °C using spectrophotometry to detect compound hydrolysis. As examples, Figure 3 shows that the absorbance maxima at 266 and 262 nm decreased over time for compounds **1** and **2**, respectively, while a new peak appeared at 226 nm, which is indicative of benzoic acid formation by *N*-benzoylpyrazole hydrolysis. Compound hydrolysis was verified by following hydrolysis of compound **1** using reverse-phase high-performance liquid chromatography (RP-HPLC). RP-HPLC traces of the progression of compound **1** hydrolysis revealed the formation of two major product peaks, one at 3.7 min and the other at 4.0 min (Figure 4). The peak eluting at 4.0 min is very close to that of pure benzoic acid ($t_R$ = 3.9 min), suggesting it is a benzoate derivative, whereas the peak at 7.7 min represents nonhydrolyzed starting material and the peak at 3.7 min likely represents the unsubstituted pyrazole, as it elutes with a retention time close to that of pure pyrazole (3.3 min). To confirm hydrolysis, compound **1** was dissolved in 85% DMSO-$d_6$/15% $D_2O$, incubated for 0 h (control) or 36 h at 37 °C, and analyzed by $^1$H NMR. Compared to the 0 h sample, two new signals at $\delta$ = 7.28 ppm and $\delta$ = 7.98 ppm were present in the 36 h sample, corresponding to protons of the hydrolytic products (*p*-fluorobenzoic acid and 4-chloropyrazole), as well as the signals of nonhydrolyzed compound **1** (see Supporting Information Table S4). Thus, these data verify that we are detecting compound hydrolysis using our spectrophotometric assay.

Using specific absorbance maxima for the other *N*-benzoylpyrazoles under investigation (Table 3), we monitored hydrolysis of the remaining set of selected compounds and used these data to create semilogarithmic plots for determining rate constants ($k'$) of spontaneous hydrolysis (see Supporting Information Figure S1 for example plots). As shown in Table 3,

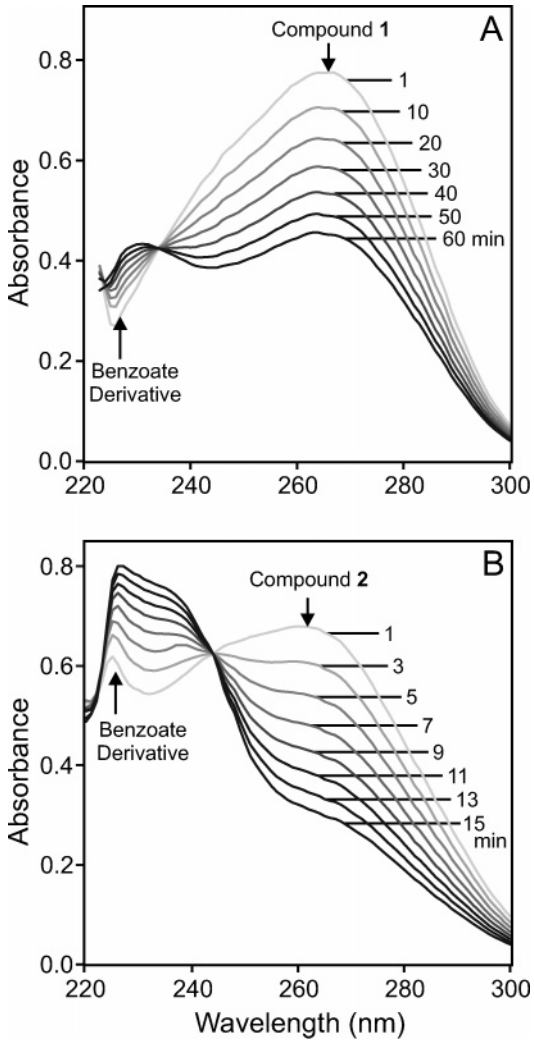


**Figure 3.** Analysis of changes in compound absorbance resulting from spontaneous hydrolysis of *N*-benzoylpyrazole derivatives. The changes in absorbance spectra of compounds **1** and **2** (20 $\mu$M in 0.05 M phosphate buffer, pH 7.3, 25 °C) were monitored over time in solution. Representative scans are from three independent experiments.

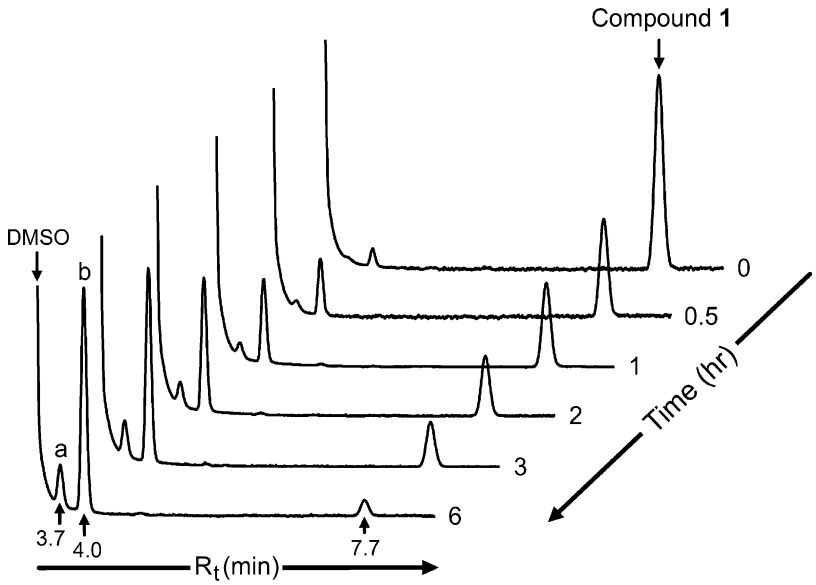


**Figure 4.** Analysis of hydrolysis of *N*-benzoylpyrazole derivatives by RP-HPLC. Changes in the chromatographic profile of compound **1** over time in solution are shown. Relevant peaks discussed in the text (a and b) are indicated. Representative chromatogram profiles are from three independent experiments.

**Table 3.** Kinetic Constants[a] for the Spontaneous Hydrolysis of Selected *N*-Benzoylpyrazoles

| compd | $\lambda$ (nm)[b] | $k'$ ($min^{-1} \times 10^3$) | $t_{1/2}$ (h) |
|---|---|---|---|
| **1** | 266 | 7.26 | 1.6 |
| **2** | 262 | 40.5 | 0.29 |
| **3** | 262 | 56.6 | 0.22 |
| **4** | 265 | 56.2 | 0.21 |
| **5** | 270 | 291.9 | 0.04 |
| **6** | 262 | 22.4 | 0.51 |
| **7** | 270 | 7.75 | 2.1 |
| **8** | 255 | 10.59 | 1.1 |
| **9** | 254 | 70.4 | 0.16 |
| **13** | 265 | 3.92 | 3.1 |
| **17** | 260 | 2.76 | 4.2 |
| **18** | 272 | 117.0 | 0.10 |
| **19** | 270 | 348.9 | 0.033 |
| **20** | 266 | 21.5 | 0.55 |
| **21** | 262 | 2.76 | 4.2 |
| **22** | 264 | 2.3 | 5.1 |
| **23** | 266 | 1.99 | 6.2 |
| **24** | 290 | 1.15 | 10.0 |
| **25** | 262 | 3.92 | 3.0 |
| **26** | 245 | 9.44 | 1.2 |
| **27** | 266 | 16.12 | 0.73 |
| **28** | 265 | 5.65 | 2.2 |
| **29** | 260 | 2.30 | 5.3 |
| **30** | 265 | 4.38 | 2.6 |
| **34** | 266 | 10.4 | 1.1 |
| **35** | 270 | 4.6 | 2.5 |
| **42** | 250 | 2.1 | 5.6 |
| **43** | 258 | 0.46 | 25.1 |
| **53** | 258 | 1.6 | 7.2 |
| **55** | 258 | 0.92 | 12.5 |
| **56** | 260 | 6.1 | 2.2 |
| **57** | 270 | 3.7 | 3.1 |
| **58** | 268 | 5.5 | 2.1 |
| **59** | 256 | 1.15 | 10.0 |

[a] The kinetic constants were obtained at pH 7.3 and 25 °C. [b] Absorption maxima that were used for monitoring spontaneous hydrolysis.

compounds **7**, **13**, **17**, **21**−**25**, and **28**−**30** were the most stable with $t_{1/2} > 2$ h. The presence of a nitro group (compounds **3**, **5**, **9**, and **18**−**20**) appears to increase the rate of spontaneous hydrolysis, with an average $t_{1/2}$ of ∼11 min for the nitropyrazoles. Nitro groups are strong electron-withdrawing moieties and have previously been reported to increase the activity of pyrazolooxadiazinone inhibitors of serine proteases.[41] Likewise, the selected nitropyrazoles were also potent NE inhibitors (Tables 1 and 2). In these compounds, the nitro substituent enhances positive charge on the carbonyl carbon atom, making it more susceptible to nucleophilic attack by a water molecule (spontaneous hydrolysis) or by the Ser195 hydroxyl group in the NE catalytic site.[42−44] Aside from the nitropyrazoles, however, there was no direct correlation between rates of spontaneous hydrolysis and anti-NE activity for the other inhibitors tested. For example, compound **7** (a potent NE inhibitor), compound **28** (a weak NE inhibitor), and inactive compound **56** all had similar rates of hydrolysis ($t_{1/2} = 2.1-2.2$ h). In general, the most potent NE inhibitors, excluding the nitropyrazoles (compounds **5**, **18**, and **19)**, were more stable than 6-acylamino-2-[1-(ethylsulfonyl)oxy]-1*H*-isoindole-1,3-diones[45] but less stable than $\beta$-lactam,[30] 1,2,5-thiadiazolidin-3-one 1,1-dioxide,[46] and 2-azetidinone[47] inhibitors of NE.

The relatively rapid rate of spontaneous hydrolysis of *N*-benzoylpyrazole inhibitors allowed us to evaluate reversibility of NE inhibition over time. As shown in Figure 5, NE was rapidly inhibited, with no lag period after addition of compound, and inhibition was maximal during the first 30 min with compounds **1**, **7**, and **18** at nanomolar concentrations (panels A, C, and E). However, inhibition by the most rapidly hydrolyzable inhibitor (compound **18**) was soon reversed, and full recovery of NE enzyme was observed after ∼7 h after treatment with up to 2 $\mu$M of the compound (Figure 5B). Indeed, subsequent addition of a more fluorogenic substrate showed that the enzyme was still active after the 7 h incubation period (indicated by arrow in Figure 5B). In comparison, reversal of inhibition by compounds **1** and **7** was much slower, and NE was still inhibited by ≥0.5 $\mu$M compounds **1** and **7** at 2 and 5 h after treatment, respectively (parts D and F of Figure 5). Thus, these results suggest that *N*-benzoylpyrazoles may be pseudoirreversible inhibitors of NE that covalently attack the enzyme active site but can be reversed by hydrolysis of the acyl−enzyme complex. Indeed, other known inhibitors of NE, such as Sivelestat (ONO-5046), utilize a similar pseudoirreversible mechanism.[48] To support this conclusion, we treated NE with a range of stable ($t_{1/2} > 2$ h) and unstable inhibitors ($t_{1/2} < 1$ h) at a relatively high concentration (25 $\mu$M), removed free inhibitor by ultrafiltration of the enzyme/inhibitor mixture, and then moni-

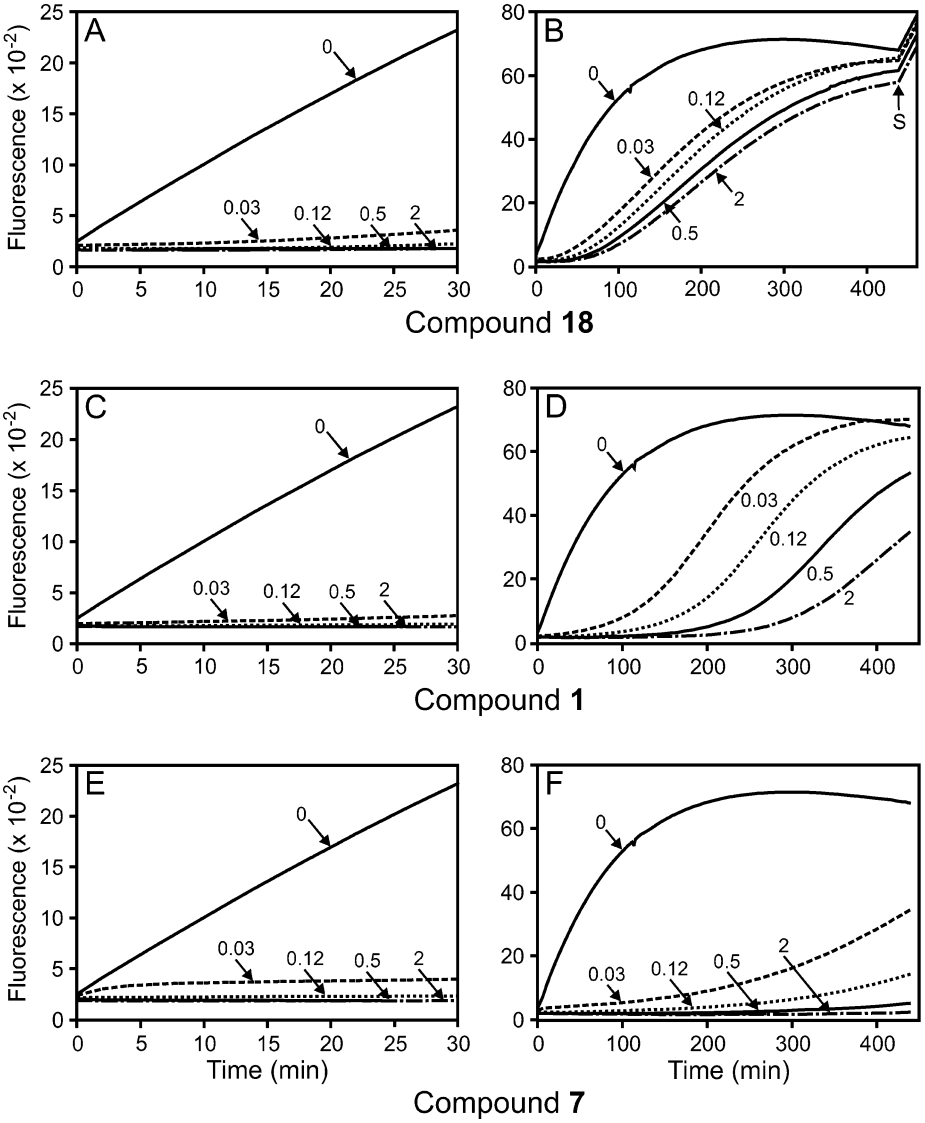


**Figure 5.** Evaluation of NE inhibition by representative *N*-benzoylpyrazole derivatives over extended periods of time. NE was incubated with the indicated compounds, and kinetic curves monitoring substrate cleavage catalyzed by NE during the first 30 min (A, C, and E) and from 0 to 7 h (B, D, and F) are shown. Representative curves are from three independent experiments.

tored recovery of NE activity over time. As shown in Figure 6, inhibition of NE by the selected inhibitors was fully reversible, although with differing kinetics between compounds. For example, inhibition by compound **20** was rapidly reversed after compound removal (<2 h for full recovery of enzymatic activity), reversal of inhibition by compound **21** was slower (~16 h), and reversal of compound **24** inhibition was very slow (>24 h). These data suggest varying degrees of stability of the enzyme−inhibitor complexes formed with individual compounds.

**Specificity of *N*-Benzoylpyrazoles.** To evaluate inhibitor specificity, we analyzed the effects of the 53 *N*-benzoylpyrazole derivatives on six different proteases other than NE. These proteases included four serine proteases [human pancreatic chymotrypsin (EC 3.4.21.1), human plasma kallikrein (EC 3.4.21.34), human thrombin (EC 3.4.21.5), and human urokinase (urokinase-type plasminogen activator precursor, EC 3.4.21.73)], a zinc-dependent protease [porcine kidney aminopeptidase M (EC 3.4.11.2)], and an aspartic protease [human spleen cathepsin D (EC 3.4.23.5)]. As shown in Table 4 and Supporting Information Table S2, none of the *N*-benzoylpyrazole derivatives inhibited aminopeptidase M and cathepsin D, and most derivatives either did not inhibit kallikrein or inhibited this enzyme

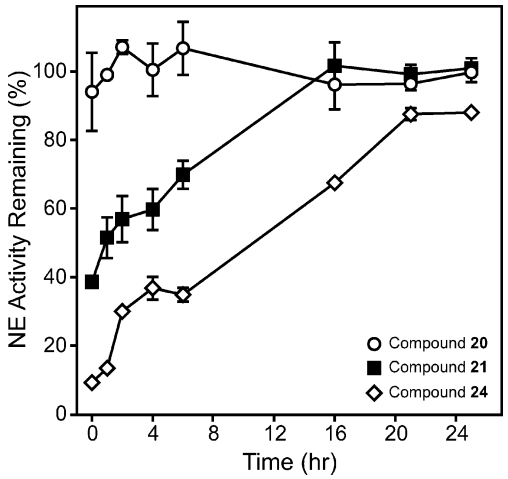


**Figure 6.** *N*-Benzoylpyrazole derivatives are reversible inhibitors of NE. NE was incubated with 25 $\mu$M of the indicated inhibitors or without inhibitor (control) in buffer A. After 15 min, excess inhibitor was removed by ultrafiltration. Control samples were treated under the same conditions. The samples were then resuspended in buffer A, and aliquots were withdrawn at the indicated times and assayed for enzyme activity. Representative curves are from two independent experiments.

**Table 4.** Analysis of *N*-Benzoylpyrazole Inhibitory Specificity[a]

| | $IC_{50}$ (nM) | | | | | |
|---|---|---|---|---|---|---|
| compd | chymotrypsin | kallikrein | thrombin | urokinase | amino-peptidase M | cathepsin D |
| **1** | 40 | 6600 | 6900 | 2500 | NI | NI |
| **2** | 15 | 11900 | 51 | 120 | NI | NI |
| **3** | 340 | 11300 | 680 | 170 | NI | NI |
| **4** | 120 | NI | 120 | 1100 | NI | NI |
| **5** | 2700 | NI | 11900 | 18200 | NI | NI |
| **6** | 57 | 12300 | 390 | 1500 | NI | NI |
| **7** | 15 | 6200 | 4700 | 1700 | NI | NI |
| **8** | 125 | 5700 | 2800 | 2600 | NI | NI |
| **9** | 1200 | 4400 | 2800 | 1500 | NI | NI |
| **13** | 1800 | NI | NI | 32300 | NI | NI |
| **17** | 50 | 42200 | 4800 | 24900 | NI | NI |
| **18** | 190 | 6100 | 4300 | 3100 | NI | NI |
| **19** | 7000 | 18800 | 11000 | 47900 | NI | NI |
| **20** | 240 | NI | 12100 | 1300 | NI | NI |
| **21** | 4700 | NI | NI | NI | NI | NI |
| **22** | 2700 | NI | NI | NI | NI | NI |
| **23** | 2300 | NI | NI | 51200 | NI | NI |
| **24** | NI | NI | NI | 33600 | NI | NI |
| **25** | 1400 | NI | NI | 18400 | NI | NI |
| **26** | NI | NI | NI | NI | NI | NI |
| **27** | 7300 | NI | NI | 28300 | NI | NI |
| **28** | 1500 | NI | NI | 4700 | NI | NI |
| **29** | 3500 | NI | NI | NI | NI | NI |
| **30** | 4700 | NI | NI | NI | NI | NI |
| **31** | 7600 | NI | NI | NI | NI | NI |
| **32** | NI | NI | NI | NI | NI | NI |
| **33** | 5600 | NI | NI | NI | NI | NI |

[a] NI: no inhibition seen at the highest concentration of compound tested (55 $\mu$M). See Supporting Information Table S2 for analysis results of compounds **34**−**59**.

at high micromolar concentrations. A few of the *N*-benzoylpyrazole derivatives inhibited thrombin (compounds **2**−**4** and **6**) or urokinase (compounds **2** and **3**) at nanomolar concentrations, whereas most of the *N*-benzoylpyrazole derivatives that were potent NE inhibitors also inhibited chymotrypsin (Table 4 and Supporting Information Table S2). This is not surprising, as NE and chymotrypsin belong to same enzyme family, and several known NE inhibitors are also relatively potent chymotrypsin inhibitors.[49,50] While enzyme selectivity between NE and chymotrypsin was low for our most potent NE inhibitors, the differential selectivity observed among this set of *N*-benzoylpyrazole derivatives suggests that differences in ring substituents ($R_1$−$R_8$) could be exploited to optimize selectivity. For example, derivatives bearing nitro groups were weaker chymotrypsin inhibitors compared to compounds with halogen or methyl substituents (Tables 1 and 2), and *N*-benzoyl-4-nitropyrazole (compound **5**), which has only a nitro group as substituent $R_2$, was a relatively selective NE inhibitor versus all other proteases tested, including chymotrypsin. Compound **24**, which is a more stable derivative ($t_{1/2}$ = 10 h), was also quite selective for NE. On the other hand, compound **54** was a potent chymotrypsin inhibitor with high selectivity versus the other proteases tested, including NE. These observations suggest that it may be possible to exploit such differences to design novel *N*-benzoylpyrazole-based inhibitors that possess both high potency and chemical stability.

**SAR Analysis and Molecular Modeling.** Analysis of the series of *N*-benzoylpyrazoles indicated that the presence or absence of ring substituents significantly affected inhibitor activity. For example, the presence of methyl groups at both the $R_1$ and $R_3$ positions decreased inhibitory activity. There were only two potent ($K_i$ < 200 nM) inhibitors (compounds **9** and **20**) among the benzoylpyrazoles with ortho substituents in the benzene ring, whereas the other 18 ortho-substituted derivatives were inactive or only weak inhibitors. Likewise, there are only

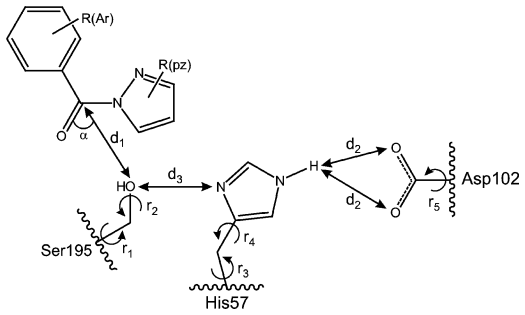


**Figure 7.** Geometric parameters important for formation of a Michaelis complex in the NE active site. The important distances (*d*) and relevant angle (α), as specified in the text, are indicated. The information is based on the model of synchronous proton transfer from the oxyanion hole in NE.[51,58]

two potent inhibitors (compounds **2** and **9**) with α-substituents ($R_3$) in the pyrazole ring. Note, however, that compound **2** also has a methylated carboxyl group and thus may differ from the other inhibitors in its coordination with the enzyme. Overall, most low-activity and inactive compounds had substituents in positions $R_3$ and/or $R_4$/$R_8$. Thus, it appears that an ortho substituent in the benzene ring and/or α-substituent in the pyrazole rings may hinder rotation of the rings that is needed to achieve optimal conformation for interaction with the active site of the enzyme.

To investigate binding of *N*-benzoylpyrazole derivatives to the NE active site and obtain insight into the differences in inhibitory activity of the various derivatives, we performed molecular modeling studies using a 23-residue model of the NE binding site that was derived from the 1.84 Å resolution crystal structure of NE complexed with a peptide chloromethyl ketone inhibitor[42] (see Experimental Section). As reported by Vergely et al.,[51] optimization of this geometry as a constituent part of whole enzyme does not lead to noticeable changes in atom positions. We imported this structure of the NE binding site into ArgusLab and performed docking studies to identify binding modes of the flexible ligands that were favorable for the interaction between the hydroxyl group of Ser195 and the carbonyl group of the benzoylpyrazole molecule. This approach is based on a number of reports showing that the mechanism of action of serine protease inhibitors containing an N−C═O fragment involves interaction between the inhibitor's carbonyl group and Ser195[46,51,52] and/or other targets in the active site.[20,50,53,54] This mechanism of interaction has been shown to involve formation of an intermediate Michaelis complex where the inhibitor carbonyl carbon atom is located 1.8−2.6 Å from the Ser195 hydroxyl oxygen (distance $d_1$ in Figure 7), while the angle of Ser195 O$\gamma$···C═O, denoted as angle α in Figure 7, is limited to 80−120°.[51,55]

The most favorable binding modes for five active (compounds **1**, **4**, **6**, **7**, and **17**) and four inactive (compounds **35**, **39**, **53**, and **54**) benzoylpyrazole derivatives were chosen from ligand docking poses lying within a 2 kcal/mol energy gap above the lowest-energy binding mode for each compound and are presented in Figure 8, Supporting Information Figure S2, and Table 5. The $d_1$ and α values show that in highly active inhibitors (compounds **1**, **4**, **6**, **7**, and **17**) the carbonyl carbon atom is slightly more accessible to the Ser195 hydroxyl oxygen, compared to inactive benzoylpyrazoles ($d_1$ = 2.98 ± 0.29 versus 3.41 ± 0.74 Å, respectively) (Table 5). Two of the inactive compounds (**53** and **54**) also had relatively short distances $d_1$; however, the Ser195 O$\gamma$···C═O angle was too acute (α = 51°), making them unfavorable for nucleophilic attack by Ser195 in the oxyanion hole (Figure 8D and F). For example, Figure 8D

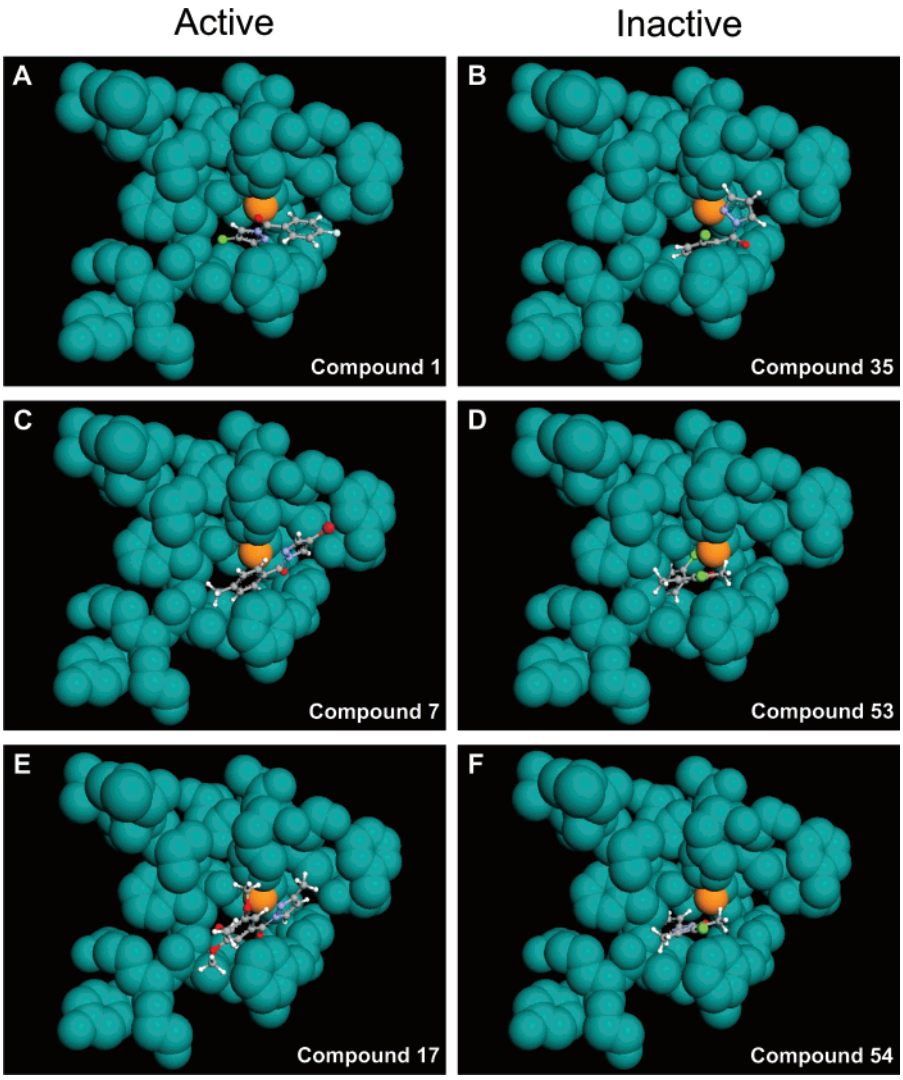


**Figure 8.** Molecular docking of active and inactive *N*-benzoylpyrazole derivatives into the binding site of NE. The NE Ser195 hydroxyl oxygen is orange. For all ligand structures, carbon is gray, hydrogen is white, nitrogen is violet, oxygen is the small red sphere, chlorine is green, fluorine is blue, and bromine is the large red sphere.

**Table 5.** Results of Docking and Subsequent Molecular Optimization for Favorable Poses[a] in the Binding Site of NE for Selected Active and Inactive *N*-Benzoylpyrazoles

| | α (deg)[b] | | distances (Å)[b] | | | | | |
|---|---|---|---|---|---|---|---|---|
| | | | | optimization | | | | |
| compd | docking | optimization | docking $d_1$ | $d_1$ | $d_2$ | $d_3$ | $L = d_{2,\min} + d_3$ | molecular deformation $\Delta E$ (kcal/mol)[c] |
| | | | | Active | | | | |
| **1** | 102 | 114 | 2.94 | 2.45 | 2.03/2.08 | 2.99 | 5.02 | 5.13 |
| **4** | 69 | 84 | 3.39 | 2.27 | 1.98/2.08 | 2.83 | 4.81 | 1.49 |
| **6** | 74 | 86 | 3.05 | 2.28 | 2.27/2.30 | 2.82 | 5.09 | 2.32 |
| **7** | 96 | 96 | 2.58 | 2.58 | 1.64/2.62 | 2.99 | 4.63 | 0 |
| **17** | 95 | 86 | 2.92 | 2.39 | 2.13/2.38 | 2.90 | 5.03 | 2.95 |
| | | | | Inactive | | | | |
| **35** | 121 | 99 | 4.14 | 2.32 | 2.71/3.97 | 3.54 | 6.25 | 2.94 |
| **39** | 92 | 103 | 3.94 | 2.67 | 3.42/3.66 | 3.57 | 6.99 | 6.60 |
| **53** | 51 | 82 | 2.64 | 2.52 | 4.23/4.96 | 4.95 | 9.18 | 11.40 |
| **54** | 51 | 80 | 2.91 | 2.40 | 2.01/2.60 | 3.28 | 5.29 | 37.36 |

[a] A docking pose was regarded as favorable if it had α and $d_1$ values closest to the optimal ranges and within 2 kcal/mol above the lowest-energy pose. [b] The angle and distances are as indicated in Figure 7. [c] Energy of molecular deformation of a selected molecule during optimization.

shows that the docked compound **53** is strongly anchored in a narrow groove of the binding site; however, rotation of the molecule to a more appropriate α angle is impossible without significantly increasing $d_1$. In support of our observations that the presence of methyl groups at $R_1$ and $R_3$ decreases inhibitor activity, the docked structure for inactive benzoylpyrazole **53** shows that the pyrazole methyl groups collide with the borders of the binding pocket and hinder penetration of molecule **53** into the oxyanion hole.

While docking studies revealed that active compounds **6** and **7** were almost planar in their favorable binding modes, with dihedral angles of ~3° between heterocycle and benzoyl ring,

the coplanarity of the two rings does not seem to correlate with high inhibitory activity. For example, the docked geometries of active inhibitors **1** and **4** are nonplanar, with dihedral angles of 48° and 51°, respectively. It is interesting to note that the user-specified, constrained planarity of molecule **35**, which contains a bulky chlorine atom in the ortho position of the phenyl ring, leads to the appearance of a "good" docking pose with $d_1 = 2.57$ Å and $\alpha = 105°$. In reality, this molecule cannot become planar, and its docking without constraints produces no binding modes suitable for the interaction with Ser195 (Figure 8B and Table 5). Thus, the presence of a large ortho substituent on the phenyl ring blocks rotation of the molecule into a conformation that can inhibit NE.

As indicated above, distances $d_1$ for NE inhibitors were generally shorter than those of their inactive analogues (Table 5). However, $d_1$ was >2.6 Å for some active compounds, which exceeds the maximum distance specified for Michaelis complex formation.[51] Most likely, this difference is due to rigidity of the binding site used in our docking study, which does not allow any degrees of freedom for Ser195 and His57, which is located in proximity to Ser195. These two residues, along with Asp102, form a conserved, active site catalytic triad that catalyzes synchronous proton transfer from Ser195 to Asp102, with His57 acting as a general base to enhance nucleophilicity of the Ser195 hydroxyl oxygen and activate the hydrolytic $H_2O$[42−44] (illustrated in Figure 7). While rotational lability of the catalytic triad residues could result in a more favorable environment for substrate binding and cleavage, certain rotational freedom could also destroy the conformationally sensitive "channel" of proton migration. To explore this issue, five torsion angles ($r_1-r_5$) in Ser195, His57, and Asp102 (Figure 7) were varied during optimization with the MM+ force field, while concurrently applying harmonic restraints to $d_1$ and $\alpha$. This approach allowed us to evaluate if rotational flexibility in Ser195, His57, and Asp102 could lead to a favorable orientation for Michaelis complex formation with an optimized ligand. Differences in the energies ($\Delta E$) of a benzoylpyrazole molecule before and after MM+ optimization within the partially flexible binding site showed that eight benzoylpyrazole derivatives (compounds **1**, **4**, **6**, **7**, **17**, **35**, **39**, and **53**) bound with suitable $d_1$ and $\alpha$ and without strong distortion of their optimal molecular geometry, as indicated by relatively low $\Delta E$ values. In addition, optimization of binding modes for these compounds did not lead to steric collisions between nonbonded atoms. Alternatively, a favorable binding mode for molecule **54** was not attainable because its penetration to Ser195 under the forces of harmonic restraints led to dramatic molecular distortion characterized by $\Delta E =$ 37.36 kcal/mol. Consequently, the lack of inhibitory activity of compound **54** can be explained by steric hindrances to formation of a Michaelis complex. The other inactive benzoylpyrazoles investigated by molecular modeling (compounds **35**, **39**, and **53**) required significant rotations $r_3$ and/or $r_4$ of His57 in order to interact with Ser195. As a result of these rotations, the distances $d_2$ and $d_3$ generally became higher than in the initial enzyme structure. The sum of the distances $L = d_2(\text{min}) + d_3$ can be regarded as the length of synchronous proton transfer between Ser195 and Asp102 (Table 5). For compound **7**, suitable $d_1$ and $\alpha$ characteristics were achieved after docking, and no further optimization was necessary. Thus, the $L$ value of 4.63 Å for compound **7** corresponds to the initial enzyme architecture. For the inactive benzoylpyrazoles (compounds **35**, **39**, and **53**), the length of proton transfer increased by 1.6−4.5 Å ($L = 7.06 \pm 1.68$), which was sufficient to interfere with general acid−base catalysis and led to loss of inhibitory activity despite the ligand being in a suitable position for Michaelis complex formation. In contrast, the active inhibitors (compounds **1**, **4**, **6**, **7**, and **17**) had shorter proton-transfer distances ($L =$ $4.92 \pm 0.2$), as well as $d_1$ and $\alpha$ values (Table 5) that favored interaction of the carbonyl group with Ser195 and enzyme inhibition.[46,51,52]

## Conclusions

We utilized HTS of a large chemical diversity library to select unique small-molecule inhibitors of NE and identified a novel class of NE inhibitors that is based on an *N*-benzoylpyrazole scaffold. A number of these compounds were highly active, with $K_i$ values of 6−300 nM, making them promising candidates for further evaluation and development. These *N*-benzoylpyrazole derivatives were competitive, pseudoirreversible inhibitors of NE activity and were relatively specific for NE and chymotrypsin, compared to a range of other proteases tested. Evaluation of compound stability in physiological buffer showed that some of the selected compounds were unstable while others were quite stable, and these differences in stability were correlated with variation in ring substituents. Clearly, the understanding of these features will be essential in future development of this class of inhibitors.

Molecular docking of the active *N*-benzoylpyrazole inhibitors to the NE catalytic site revealed favorable binding for Michaelis complex formation. Furthermore, the carbonyl group of the bound inhibitor was positioned in the oxyanion hole of the NE binding site with a favorable orientation for the interaction with the catalytic triad. In contrast, inactive benzoylpyrazoles either had unfavorable orientation for nucleophilic attack by Ser195 or were sterically hindered from optimal binding. Overall, our molecular docking and SAR analyses provide key details that could be exploited in the development of *N*-benzoylpyrazole analogues, and we suggest that the *N*-benzoylpyrazole scaffold represents a novel direction for developing NE inhibitors that exhibit high enzyme selectivity and potency.

## Experimental Section

**Compounds and Reagents.** The ActiProbe-10K chemical diversity set was obtained from TimTec, Inc. (Newark, DE). This commercial library is comprised of a random selection of 10 000 druglike compounds. Additional *N*-benzoylpyrazole derivatives were selected from the Actimol database and purchased from TimTec. The purity of the most active target compounds was confirmed by dissolving compounds directly in acetonitrile/$H_2O$ (60/40 or 65/35, v/v) and analyzing immediately by RP-HPLC, as described below. All target compounds eluted as a single peak and were found to be >98% pure (Supporting Information Table S3). Compound identity was verified by $^1$H NMR analysis at 200, 300, or 500 MHz using Bruker AC200, AC300, or Avance NMR spectrometers (Bruker BioSpin, Billerica, MA), respectively, at 23 or 30 °C and with the samples dissolved in deuterated dimethyl sulfoxide (DMSO-$d_6$) (Supporting Information Table S4; NMR analyses were preformed by TimTec, Inc.). NE, human chymotrypsin, human kallikrein, human thrombin, human urokinase, porcine aminopeptidase, and human cathepsin D as well as their substrates were purchased from Calbiochem (San Diego, CA). DMSO, DMSO-$d_6$, deuterated water ($D_2O$), pyrazole, and benzoic acid were purchased from Sigma Chemical Co. (St. Louis, MO). HPLC grade acetonitrile was from EMD Chemicals (Gibbstown, NJ), and HPLC grade $H_2O$ and trifluoroacetic acid (TFA) were from Mallinckrodt Baker Inc. (Phillipsburg, NJ).

**Library Screening and Kinetic Measurements.** We used HTS to screen the compound library for hits with NE inhibitory activity. Stock compounds were dissolved in 100% DMSO at a concentration of 2 mg/mL. The final concentration of DMSO in the reactions was 1%, and this level of DMSO had no effect on enzyme activity.

HTS was performed in black flat-bottom 96-well microtiter plates. Briefly, a solution containing buffer A (200 mM Tris-HCl, pH 7.5, 0.01% bovine serum albumin, and 0.05% Tween-20) and up to 20 mU/mL of NE (Calbiochem) was added to wells containing 20 $\mu$g/mL of each compound. The reaction was initiated by addition of 25 $\mu$M elastase substrate (*N*-methylsuccinyl-Ala−Ala-Pro-Val-7-amino-4-methylcoumarin, Calbiochem) in a final reaction volume of 100 $\mu$L/well. Kinetic measurements were obtained every 30 s for 10 min at 25 °C using a Fluoroskan Ascent FL fluorescence microplate reader (Thermo Electron, MA) with excitation and emission wavelengths at 355 and 460 nm, respectively.

For selected lead compounds, the inhibition constant ($K_i$) values were determined using Dixon plots of three to four different concentrations of the substrate.[35] At each substrate concentration, rates were determined with four to five different inhibitor concentrations, and the inverse of the velocities was plotted against the final inhibitor concentration. $K_i$ was determined from the intersection of the plotted lines ($R^2 > 0.98$ for each line).

Reactivation of the NE−inhibitor complex was investigated as reported previously.[46] Briefly, NE (20 mU/mL) was incubated with excess inhibitor at final concentrations of 25 $\mu$M in 2 mL of buffer A. After 20 min, a 50 $\mu$L aliquot was removed and assayed to verify complete inhibition of NE enzymatic activity. Excess inhibitor was removed via Centricon-10 filtration by centrifuging at 5000*g* for 1 h at 5 °C, adding 2 mL of buffer A to the retentate, and centrifuging again under the same conditions. This process was repeated again, and the final retentate was suspended in 1.5 mL of buffer A at 25 °C. At the indicated times, 50 $\mu$L aliquots were removed and added to microplate wells containing 25 $\mu$M of the fluorogenic NE substrate dissolved in 50 $\mu$L of buffer A. A control containing NE (20 mU/mL) and 0.25% DMSO was run under the same conditions.

**Analysis of Compound Stability.** Spontaneous hydrolysis of selected *N*-benzoylpyrazoles was evaluated at 25 °C in 0.05 M phosphate buffer, pH 7.3. Kinetics of *N*-benzoylpyrazole hydrolysis was monitored by measuring changes in absorbance spectra over incubation time using a SpectraMax Plus microplate spectrophotometer (Molecular Devices, Sunnyvale, CA). Absorbance ($A_t$) at the characteristic absorption maxima of each *N*-benzoylpyrazole was measured at the indicated times until no further absorbance decreases occurred ($A_\infty$).[56] Using these measurements, we created semilogarithmic plots of $\log(A_t - A_\infty)$ vs time (see Supporting Information Figure S1), and $k'$ values were determined from the slopes of these plots. Half-conversion times were calculated using $t_{1/2} = 0.693/k'$.

For selected compounds, the kinetics of hydrolysis was also confirmed by RP-HPLC. Reactions were initiated by addition of 2 $\mu$L from a 10 mM stock solution (in DMSO) of the respective compound to 200 $\mu$L of 0.05 M phosphate buffer (pH 7.3) at 25 °C. At the indicated times, aliquots (5 $\mu$L) were separated by RP-HPLC on an automated HPLC system (Shimadzu, Torrance, CA) with a Phenomenex Jupiter C18 300A column (5 $\mu$m, 25 cm × 0.46 cm) eluted with acetonitrile/water (60%/40%, v/v) containing 0.1% (v/v) TFA at a flow rate of 1 mL/min at 25 °C. The elution was monitored using a diode array detector (Shimadzu SPD-M10A VP) set to spectrum max plot (wavelength at which the highest absorbance occurs) in the region of 200−300 nm.

To verify compound hydrolysis, compound **1** was dissolved in 85% DMSO-$d_6$/15% $D_2O$ (3 mg/mL). The mixture was incubated for 36 h at 37 °C, and the samples were analyzed by $^1$H NMR on a Bruker DRX-500 spectrometer (Bruker BioSpin, Billerica, MA). Control samples were dissolved in mixture of 85% DMSO-$d_6$/15% $D_2O$ and analyzed immediately. $^1$H NMR spectra were recorded at 20 °C using 3-(trimethylsilyl)propionic-2,2,3,3-$d_4$ acid sodium salt as an internal reference.

**Analysis of Inhibitor Specificity.** Selected compounds were evaluated for their ability to inhibit a range of proteases in 100 $\mu$L reaction volumes at 25 °C. Analysis of chymotrypsin inhibition was performed in reaction mixtures containing 0.05 M Tris-HCl, pH 8.0, 30 nM human pancreas chymotrypsin, test compounds, and 100 $\mu$M substrate (Suc-Ala−Ala-Pro-Phe-7-amino-4-methylcoumarin). Thrombin inhibition was evaluated in reaction mixtures containing 0.25 M sodium phosphate, pH 7.0, 0.2 M NaCl, 0.1% PEG 8000, 1.7 U human plasma thrombin, test compounds, and 20 $\mu$M substrate (benzoyl-Phe-Val-Arg-7-amino-4-methylcoumarin). Analysis of kallikrein inhibition was performed in reaction mixtures containing 0.05 M Tris-HCl, pH 8.0, 0.1 M NaCl, 0.05% Tween-20, 2 nM human plasma kallikrein, test compounds, and 50 $\mu$M substrate (benzyloxycarbonyl-Phe-Arg-7-amino-4-methylcoumarin). Analysis of urokinase inhibition assay was performed in reaction mixtures containing 0.1 M Tris-HCl, pH 8.0, 30 U/mL human urine urokinase, test compounds, and 30 $\mu$M substrate (benzyloxycarbonyl-Gly-Gly-Arg-7-amino-4-methylcoumarin). Aminopeptidase M inhibition was determined in reaction mixtures contained 0.1 M Tris-HCl, pH 7.0, 0.05% Tween-20, 2 mU porcine kidney aminopeptidase M, test compounds, and 0.4 mM substrate (L-alanyl-*p*-nitroanilide). Analysis of cathepsin D inhibition was performed in reaction mixtures containing 0.1 M sodium acetate, pH 5.0, 0.1 U/mL human spleen cathepsin D, test compounds, and 5 $\mu$M substrate (MOCAc-Gly-Lys-Pro-Ile-Leu-Phe-Phe-Arg-Leu-Lys(Dnp)-D-Arg-$NH_2$). Reactions for aminopeptidase M activity were monitored at 405 nm using a SpectraMax Plus microplate reader. Cathepsin D assays were monitored with a Fluoroskan Ascent FL microtiter plate reader at excitation and emission wavelengths of 340 and 390 nm, respectively. For all serine proteases (chymotrypsin, thrombin, kallikrein, and urokinase) activity was monitored at excitation and emission wavelengths of 355 and 460 nm, respectively. For all compounds tested, the concentration of inhibitor that causes 50% inhibition of the enzymatic reaction ($IC_{50}$) was calculated by plotting % inhibition vs logarithm of inhibitor concentration (at least six points), and the data are the mean values of at least three experiments with relative standard deviations of <15%.

**Molecular Modeling.** For computer-assisted molecular modeling we employed HyperChem, version 7.0 (Hypercube, Inc., Waterloo, ON, Canada) and ArgusLab 4.0.1 (Planaria Software LLC, Seattle, WA). Molecular structures of *N*-benzoylpyrazole derivatives **1**, **4**, **6**, **7**, **17**, **35**, **39**, **53**, and **54** were first created and optimized by HyperChem with the use of the molecular mechanics MM+ force field. These structures were then subjected to docking computations by ArgusLab with AScore scoring functions[57] to find the lowest-energy binding modes. Flexibility of an inhibitor was accounted for around all rotatable bonds automatically identified by ArgusLab. The binding site of NE was considered to be rigid in the docking procedure, and its geometry was obtained by downloading a crystal structure of NE complexed with a peptide chloromethyl ketone inhibitor[42] from the Protein Data Bank (code 1HNE). Amino acid residues within 7 Å of any non-hydrogen atom of the inhibitor were regarded as belonging to the binding site, and 22 residues satisfied this condition (Phe41, Cys42, Ala55, His57, Cys58, Leu99B, Asp102, Val190, Cys191, Phe192, Gly193, Asp194, Ser195, Gly196, Ser197, Ala213, Ser214, Phe215, Val216, Arg217A, Gly218, and Tyr224). Although Ala56 is 8.3 Å away from the nearest inhibitor atom, we included Ala55 in the binding site to maintain continuous sequence from Ala55 to Cys58. We then removed the chloromethyl ketone inhibitor and cocrystallized water molecules to obtain the 23-residue model of the NE binding site that was used for docking.

Binding modes found for each inhibitor within a 2 kcal/mol gap above the lowest-energy mode were examined for the potential to form a Michaelis complex between the hydroxyl group of Ser195 and the inhibitor's carbonyl group, and values of $d_1$ and $\alpha$ (Figure 7) were determined for each docked compound. These modes were further optimized by molecular mechanics with the MM+ force field using HyperChem. During this optimization, we varied torsion angles $r_1-r_5$ in Ser195, His57, and Asp102 and also applied harmonic restraints to $d_1$ and $\alpha$. Energy terms for the restraints were calculated as $E_d = K_d(d_1 - 1.5)^2$ and $E_\alpha = K_\alpha(\alpha - 100°)$,[2] where $K_d = 15$ kcal·mol$^{-1}$·Å$^{-1}$ and $K_\alpha = 3$ kcal·mol$^{-1}$·deg$^{-1}$. These restraints served as driving forces to attain the conditions of Michaelis complex formation through simultaneous cooperative movements of key residues within the binding site. Again, values of $d_1$ and $\alpha$ were determined, as well as distances $d_2$ and $d_3$ (Figure

7). The distance $d_2$ is measured between the NH hydrogen in the His57 imidazole ring and either one of the carboxylic oxygens in Asp102. It defines the synchronous proton transfer from the oxyanion hole.[58] The distance between the hydroxyl proton in Ser195 and the basic pyridine-type nitrogen in His57 is also important for this transfer. However, because of easy rotation of the hydroxyl about the C−O bond in Ser195, we measured $d_3$ between the oxygen in Ser195 and the basic nitrogen in His57 (see Figure 7).

Molecular mechanics optimization of a binding mode also caused deformation of the benzoylpyrazole molecule, and the change in energy ($\Delta E$) due to deformation was calculated as $\Delta E = E_2 - E_1$, where $E_1$ is the MM+ conformational energy of the inhibitor molecule in the docked structure chosen as the favorable binding mode and where $E_2$ is the conformational energy of the inhibitor in its geometry attained in the optimized docked structure.

**Acknowledgment.** We thank Dr. Scott Busse from the Department of Chemistry and Biochemistry at Montana State University for providing expert NMR analysis. This work was supported in part by Department of Defense Grant W9113M-04-1-0001, National Institutes of Health Grant RR020185, and the Montana State University Agricultural Experimental Station. The U.S. Army Space and Missile Defense Command, 64 Thomas Drive, Frederick, MD 21702, is the awarding and administering acquisition office. The content of this report does not necessarily reflect the position or policy of the U.S. Government.

**Supporting Information Available:** Table S1 on the effect of *N*-benzoylpyrazoles **34**−**59** on NE activity, Table S2 on the analysis of inhibitory specificity for compounds **34**−**59**; Table S3 on the HPLC analysis of selected compounds, Table S4 on the $^1$H NMR analysis of selected compounds, Figure S1 showing examples of semilogarithmic plots used to determine rate constants for *N*-benzoylpyrazole spontaneous hydrolysis, and Figure S2 showing further examples of molecular docking of *N*-benzoylpyrazoles into the active site of NE. This material is available free of charge via the Internet at http://pubs.acs.org.

## References

(1) Mannino, D. M. Epidemiology and global impact of chronic obstructive pulmonary disease. *Semin. Respir. Crit. Care Med.* **2005**, *26*, 204−210.
(2) Rubenfeld, G. D.; Herridge, M. S. Epidemiology and outcomes of acute lung injury. *Chest* **2007**, *131*, 554−562.
(3) Strausbaugh, S. D.; Davis, P. B. Cystic fibrosis: a review of epidemiology and pathobiology. *Clin. Chest Med.* **2007**, *28*, 279−288.
(4) Abraham, E. Neutrophils and acute lung injury. *Crit. Care Med.* **2003**, *31*, S195−S199.
(5) Moraes, T. J.; Zurawska, J. H.; Downey, G. P. Neutrophil granule contents in the pathogenesis of lung injury. *Curr. Opin. Hematol.* **2006**, *13*, 21−27.
(6) Pham, C. T. Neutrophil serine proteases: specific regulators of inflammation. *Nat. Rev. Immunol.* **2006**, *6*, 541−550.
(7) Faurschou, M.; Borregaard, N. Neutrophil granules and secretory vesicles in inflammation. *Microbes Infect.* **2003**, *5*, 1317−1327.
(8) Stockley, R. A. Neutrophils and protease/antiprotease imbalance. *Am. J. Respir. Crit. Care Med.* **1999**, *160*, S49−S52.
(9) Kawabata, K.; Hagio, T.; Matsuoka, S. The role of neutrophil elastase in acute lung injury. *Eur. J. Pharmacol.* **2002**, *451*, 1−10.
(10) Moraes, T. J.; Chow, C.-W.; Downey, G. P. Proteases and lung injury. *Crit. Care Med.* **2003**, *31*, S189−S194.
(11) Owen, C. A.; Campbell, E. J. The cell biology of leukocyte-mediated proteolysis. *J. Leukocyte Biol.* **1999**, *65*, 137−150.
(12) Chua, F.; Laurent, G. J. Neutrophil elastase: mediator of extracellular matrix destruction and accumulation. *Proc. Am. Thorac. Soc.* **2006**, *3*, 424−427.
(13) Dollery, C. M.; Owen, C. A.; Sukhova, G. K.; Krettek, A.; Shapiro, S. D.; Libby, P. Neutrophil elastase in human atherosclerotic plaques: production by macrophages. *Circulation* **2003**, *107*, 2829−2836.
(14) Bedard, M.; McClure, C. D.; Schiller, N. L.; Francoeur, C.; Cantin, A.; Denis, M. Release of interleukin-8, interleukin-6, and colony-stimulating factors by upper airway epithelial cells: implications for cystic fibrosis. *Am. J. Respir. Cell Mol. Biol.* **1993**, *9*, 455−462.
(15) Fitch, P. M.; Roghanian, A.; Howie, S. E.; Sallenave, J. M. Human neutrophil elastase inhibitors in innate and adaptive immunity. *Biochem. Soc. Trans.* **2006**, *34*, 279−282.
(16) Carden, D.; Xiao, F.; Moak, C.; Willis, B. H.; Robinson-Jackson, S.; Alexander, S. Neutrophil elastase promotes lung microvascular injury and proteolysis of endothelial cadherins. *Am. J. Physiol.* **1998**, *275*, H385−H392.
(17) Barnes, P. J.; Stockley, R. A. COPD: current therapeutic interventions and future approaches. *Eur. Respir. J.* **2005**, *25*, 1084−1106.
(18) Kardos, P.; Keenan, J. Tackling COPD: a multicomponent disease driven by inflammation. *Med. Gen. Med.* **2006**, *8*, 54.
(19) Chughtai, B.; O'Riordan, T. G. Potential role of inhibitors of neutrophil elastase in treating diseases of the airway. *J. Aerosol Med.* **2004**, *17*, 289−298.
(20) Tremblay, G. M.; Janelle, M. F.; Bourbonnais, Y. Anti-inflammatory activity of neutrophil elastase inhibitors. *Curr. Opin. Invest. Drugs* **2003**, *4*, 556−565.
(21) Moreira, R.; Santana, A. B.; Iley, J.; Neres, J.; Douglas, K. T.; Horton, P. N.; Hursthouse, M. B. Design, synthesis, and enzymatic evaluation of N1-acyloxyalkyl- and N1-oxazolidin-2,4-dion-5-yl-substituted beta-lactams as novel inhibitors of human leukocyte elastase. *J. Med. Chem.* **2005**, *48*, 4861−4870.
(22) Odagaki, Y.; Ohmoto, K.; Matsuoka, S.; Hamanaka, N.; Nakai, H.; Toda, M.; Katsuya, Y. The crystal structure of the complex of non-peptidic inhibitor of human neutrophil elastase ONO-6818 and porcine pancreatic elastase. *Bioorg. Med. Chem.* **2001**, *9*, 647−651.
(23) Veale, C. A.; Bernstein, P. R.; Bohnert, C. M.; Brown, F. J.; Bryant, C.; Damewood, J. R., Jr.; Earley, R.; Feeney, S. W.; Edwards, P. D.; Gomes, B.; Hulsizer, J. M.; Kosmider, B. J.; Krell, R. D.; Moore, G.; Salcedo, T. W.; Shaw, A.; Silberstein, D. S.; Steelman, G. B.; Stein, M.; Strimpler, A.; Thomas, R. M.; Vacek, E. P.; Williams, J. C.; Wolanin, D. J.; Woolson, S. Orally active trifluoromethyl ketone inhibitors of human leukocyte elastase. *J. Med. Chem.* **1997**, *40*, 3173−3181.
(24) Doherty, J. B.; Ashe, B. M.; Argenbright, L. W.; Barker, P. L.; Bonney, R. J.; Chandler, G. O.; Dahlgren, M. E.; Dorn, C. P., Jr.; Finke, P. E.; Firestone, R. A.; Fletcher, D.; Hagmann, W. K.; Mumord, R.; O'Grady, L.; Maycock, A. L.; Pisano, J. M.; Shah, S. K.; Thompson, K. R.; Zimmerman, M. Cephalosporin antibiotics can be modified to inhibit human leukocyte elastase. *Nature* **1986**, *322*, 192−194.
(25) Edwards, P. D.; Bernstein, P. R. Synthetic inhibitors of elastase. *Med. Res. Rev.* **1994**, *14*, 127−194.
(26) Macdonald, S. J.; Dowle, M. D.; Harrison, L. A.; Clarke, G. D.; Inglis, G. G.; Johnson, M. R.; Shah, P.; Smith, R. A.; Amour, A.; Fleetwood, G.; Humphreys, D. C.; Molloy, C. R.; Dixon, M.; Godward, R. E.; Wonacott, A. J.; Singh, O. M.; Hodgson, S. T.; Hardy, G. W. Discovery of further pyrrolidine trans-lactams as inhibitors of human neutrophil elastase (HNE) with potential as development candidates and the crystal structure of HNE complexed with an inhibitor (GW475151). *J. Med. Chem.* **2002**, *45*, 3878−3890.
(27) McBride, J. D.; Freeman, H. N.; Leatherbarrow, R. J. Selection of human elastase inhibitors from a conformationally constrained combinatorial peptide library. *Eur. J. Biochem.* **1999**, *266*, 403−412.
(28) Cheng, D. H.; Shen, Q.; Qian, J.; Qian, Z.; Ye, Q. Z. Expression and purification of catalytic domain of human macrophage elastase for high throughput inhibitor screening. *Acta Pharmacol. Sin.* **2002**, *23*, 143−151.
(29) Gao, F.; Du, G. H. Application of chemical arrays in screening elastase inhibitors. *Comb. Chem. High Throughput Screening* **2006**, *9*, 381−388.
(30) Knight, W. B.; Green, B. G.; Chabin, R. M.; Gale, P.; Maycock, A. L.; Weston, H.; Kuo, D. W.; Westler, W. M.; Dorn, C. P.; Finke, P. E.; Hagmann, W. K.; Hale, J. J.; Liesch, J.; MacCoss, M.; Navia, M. A.; Shah, S. K.; Underwood, D.; Doherty, J. B. Specificity, stability, and potency of monocyclic $\beta$-lactam inhibitors of human leucocyte elastase. *Biochemistry* **1992**, *31*, 8160−8170.
(31) Schepetkin, I. A.; Khlebnikov, A. I.; Kirpotina, L. N.; Quinn, M. T. Novel small-molecule inhibitors of anthrax lethal factor identified by high-throughput screening. *J. Med. Chem.* **2006**, *49*, 5232−5244.
(32) Schepetkin, I. A.; Kirpotina, L. N.; Khlebnikov, A. I.; Quinn, M. T. High-throughput screening for small-molecule activators of neutrophils: identification of novel *N*-formyl peptide receptor agonists. *Mol. Pharmacol.* **2007**, *71*, 1061−1074.
(33) McGovern, S. L.; Caselli, E.; Grigorieff, N.; Shoichet, B. K. A common mechanism underlying promiscuous inhibitors from virtual and high-throughput screening. *J. Med. Chem.* **2002**, *45*, 1712−1722.

(34) Blanchard, J. E.; Elowe, N. H.; Huitema, C.; Fortin, P. D.; Cechetto, J. D.; Eltis, L. D.; Brown, E. D. High-throughput screening identifies inhibitors of the SARS coronavirus main proteinase. *Chem. Biol.* **2004**, *11*, 1445−1453.
(35) Dixon, M. The determination of enzyme inhibitor constants. *Biochem. J.* **1953**, *55*, 170−171.
(36) Kakiuchi, N.; Nishikawa, S.; Hattori, M.; Shimotohno, K. A high throughput assay of the hepatitis C virus nonstructural protein 3 serine proteinase. *J. Virol. Methods* **1999**, *80*, 77−84.
(37) Pomarnacka, E.; Angielski, S.; Hoppe, A. Derivatives of 4-chloro-5-sulfamoylbenzoic acid. 8. Synthesis and diuretic activity of pyrazole [3,2-B] quinazoline and 1-benzoylpyrazole derivatives. *Acta Pol. Pharm.* **1984**, *41*, 141−151.
(38) Wright, J. B.; Dulin, W. E.; Markillie, J. H. The antidiabetic activity of 3,5-dimethylpyrazoles. *J. Med. Chem.* **1964**, *7*, 102−105.
(39) Goodell, J. R.; Puig-Basagoiti, F.; Forshey, B. M.; Shi, P. Y.; Ferguson, D. M. Identification of compounds with anti-West Nile virus activity. *J. Med. Chem.* **2006**, *49*, 2127−2137.
(40) Paintz, M.; Bekemeier, H.; Metzner, J.; Wenzel, U. Pharmacological activities of a homologous series of pyrazole derivatives including quantitative structure−activity relationships (QSAR). *Agents Actions, Suppl.* **1982**, *10*, 47−58.
(41) Vicentini, C. B.; Guarneri, M.; Andrisano, V.; Guccione, S.; Langer, T.; Marschhofer, R.; Chabin, R.; Edison, A. M.; Huang, X.; Knight, W. B.; Giori, P. Potential of pyrazolooxadiazinone derivatives as serine protease inhibitors. *J. Enzyme Inhib.* **2001**, *16*, 15−34.
(42) Navia, M. A.; McKeever, B. M.; Springer, J. P.; Lin, T. Y.; Williams, H. R.; Fluder, E. M.; Dorn, C. P.; Hoogsteen, K. Structure of human neutrophil elastase in complex with a peptide chloromethyl ketone inhibitor at 1.84-Å resolution. *Proc. Natl. Acad. Sci. U.S.A.* **1989**, *86*, 7−11.
(43) Dodson, G.; Wlodawer, A. Catalytic triads and their relatives. *Trends Biochem. Sci.* **1998**, *23*, 347−352.
(44) Katona, G.; Wilmouth, R. C.; Wright, P. A.; Berglund, G. I.; Hajdu, J.; Neutze, R.; Schofield, C. J. X-ray structure of a serine protease acyl−enzyme complex at 0.95-Å resolution. *J. Biol. Chem.* **2002**, *277*, 21962−21970.
(45) Vagnoni, L. M.; Gronostaj, M.; Kerrigan, J. E. 6-Acylamino-2−1(ethylsulfonyl)oxy]-1*H*-isoindole-1,3-diones mechanism-based inhibitors of human leukocyte elastase and cathepsin G: effect of chirality in the 6-acylamino substituent on inhibitory potency and selectivity. *Bioorg. Med. Chem.* **2001**, *9*, 637−645.
(46) Groutas, W. C.; Kuang, R.; Venkataraman, R.; Epp, J. B.; Ruan, S.; Prakash, O. Structure-based design of a general class of mechanism-based inhibitors of the serine proteinases employing a novel amino acid-derived heterocyclic scaffold. *Biochemistry* **1997**, *36*, 4739−4750.
(47) Clemente, A.; Domingos, A.; Grancho, A. P.; Iley, J.; Moreira, R.; Neres, J.; Palma, N.; Santana, A. B.; Valente, E. Design, synthesis and stability of *N*-acyloxymethyl- and *N*-aminocarbonyloxymethyl-2-azetidinones as human leukocyte elastase inhibitors. *Bioorg. Med. Chem. Lett.* **2001**, *11*, 1065−1068.
(48) Ohbayashi, H. Neutrophil elastase inhibitors as treatment for COPD. *Expert. Opin. Invest. Drugs* **2002**, *11*, 965−980.
(49) Veale, C. A.; Bernstein, P. R.; Bryant, C.; Ceccarelli, C.; Damewood, J. R., Jr.; Earley, R.; Feeney, S. W.; Gomes, B.; Kosmider, B. J.; Steelman, G. B. Nonpeptidic inhibitors of human leukocyte elastase. 5. Design, synthesis, and X-ray crystallography of a series of orally active 5-aminopyrimidin-6-one-containing trifluoromethyl ketones. *J. Med. Chem.* **1995**, *38*, 98−108.
(50) Walker, B.; Lynas, J. F. Strategies for the inhibition of serine proteases. *Cell. Mol. Life Sci.* **2001**, *58*, 596−624.
(51) Vergely, I.; Laugaa, P.; Reboud-Ravaux, M. Interaction of human leukocyte elastase with a *N*-aryl azetidinone suicide substrate: conformational analyses based on the mechanism of action of serine proteinases. *J. Mol. Graphics* **1996**, *14*, 145, 158−167.
(52) Aoyama, Y.; Uenaka, M.; Konoike, T.; Hayasaki-Kajiwara, Y.; Naya, N.; Nakajima, M. Inhibition of serine proteases: activity of 1,3-diazetidine-2,4-diones. *Bioorg. Med. Chem. Lett.* **2001**, *11*, 1691−1694.
(53) Metz, W. A.; Peet, N. P. Inhibitors of human neutrophil elastase as a potential treatment for inflammatory diseases. *Expert Opin. Ther. Pat.* **1999**, *9*, 851−868.
(54) Nakayama, Y.; Odagaki, Y.; Fujita, S.; Matsuoka, S.; Hamanaka, N.; Nakai, H.; Toda, M. Clarification of mechanism of human sputum elastase inhibition by a new inhibitor, ONO-5046, using electrospray ionization mass spectrometry. *Bioorg. Med. Chem. Lett.* **2002**, *12*, 2349−2353.
(55) Burgi, H. B.; Dunitz, J. D.; Lehn, J. M.; Wipff, G. Stereochemistry of reaction paths at carbonyl centers. *Tetrahedron* **1974**, *30*, 1563−1572.
(56) Forist, A. A.; Weber, D. J. Kinetics of hydrolysis of hypoglycemic 1-acyl 3,5-dimethylpyrazoles. *J. Pharm. Sci.* **1973**, *62*, 318−319.
(57) Morris, G. M.; Goodsell, D. S.; Halliday, R. S.; Huey, R.; Hart, W. E.; Belew, R. K.; Olson, A. J. Automated docking using a Lamarckian genetic algorithm and an empirical binding free energy function. *J. Comput. Chem.* **1998**, *19*, 1639−1662.
(58) Peters, M. B.; Merz, K. M. Semiempirical comparative binding energy analysis (SE-COMBINE) of a series of trypsin inhibitors. *J. Chem. Theory Comput.* **2006**, *2*, 383−399.

JM070600+